Proceedings of the 30th Symposium of the International Committee on Aeronautical Fatigue, June 2-7, 2019, Krakow, Poland
DOI: 10.1007/978-3-030-21503-3_3

30th ICAF Symposium – Kraków, 2 – 7 June 2019

High Cycle Fatigue and Fatigue Crack Growth Rate in Additive Manufactured Titanium Alloys

Xiang Zhang [1], Abdul Khadar Syed [1], Romali Biswal [1]
Filomeno Martina [2], Jialuo Ding [2], Stewart Williams [2]

[1] Research Centre for Manufacturing and Materials Engineering, Coventry University, Coventry, CV1 5FB, UK

[2] Welding Engineering and Laser Processing Centre, Cranfield University, Cranfield, MK43 0AL, UK
Corresponding author email address: xiang.zhang@coventry.ac.uk

ABSTRACT

The Wire + Arc Additive Manufacture (WAAM) process can produce large metal parts in the metre scale, at much higher deposition rate and more efficient material usage compared to the powder bed fusion additive manufacturing (AM) processes. WAAM process also offers lead time reduction and much lower buy-to-fly ratio compared to traditional process methods, e.g. forgings. Research is much needed in the areas of fatigue and fracture performance for qualification and certification of additive manufactured aircraft components.

In this study, specimens made of WAAM Ti-6Al-4V alloy were tested and analysed focusing on two key areas of structural integrity and durability:

(1) High cycle fatigue and effect of defects: crack initiation at porosity defects was investigated via fatigue and interrupted fatigue-tomography testing performed on specimens with porosity defects purposely embedded in the specimen gauge section. Key findings are as follows. Presence of porosity did not affect the tensile strengths, however both ductility and fatigue strength were significantly reduced. Fatigue life could not be correlated by the applied stress, e.g. in terms of the *S-N* curves, owing to the different pore sizes. Using the fracture mechanics approach and Murakami's stress intensity factor equation for pores, good correlation was found between the fatigue life and stress intensity factor range of the crack initiating defects. Predictive methods for fatigue strength reduction were developed taking account of the defect size, location, and distribution.

(2) Fatigue crack growth rate: effect of heterogeneous microstructure was investigated via two different material deposition methods and testing two crack orientations. Fatigue crack growth rates were measured for damage tolerance design considerations. Unique microstructure features and their effect on the property anisotropy are discussed.

Keywords: Additive manufacturing, porosity defects, fatigue crack initiation, fatigue crack growth rate

Published by Springer. This is the Author Accepted Manuscript issued with: Creative Commons Attribution Non-Commercial License (CC:BY:NC 4.0).
The final published version (version of record) is available online at DOI:10.1007/978-3-030-21503-3_3. Please refer to any applicable publisher terms of use.

INTRODUCTION

Wire + Arc Additive Manufacturing (WAAM) is a novel process where a wire is fed through an electric or plasma arc at a constant rate to build a near net shape part. WAAM titanium alloy Ti-6Al-4V has found its applications in the aerospace industry to produce large parts at high deposition rate, affordable cost, and much reduced lead time comparing to the traditional manufacturing and the powder bed fusion AM processes (Williams *et al.,* 2016). WAAM Ti-6Al-4V parts is practically defect-free, i.e. material density is 99.99%. However, it is recognised that feedstock contamination may occur during the wire production and/or part building process that can lead to process induced porosity defects (Wang *et al.*, 2013). In addition, complex thermal cycles and directional solidification during the WAAM process result in non-conventional microstructure and texture.

High cycle fatigue properties of WAAM Ti-6Al-4V produced by single bead deposition method showed a 10% longer fatigue life compared to the mill annealed Ti-6Al-4V (Wang *et al.*, 2013). Vertical build samples (loading axis parallel to the AM build direction) showed better fatigue properties (Wang *et al.*, 2013). The lower fatigue strength of the horizontal samples (loading axis perpendicular to the build direction) is due to the premature crack initiation from the residual porosity (Wang *et al.*, 2013). Presence of defects and non-conventional microstructure will also influence the fatigue performance and may limit the industrial adoption process of WAAM processed materials. So far, fewer studies have been done on the effects of porosity and non-conventional microstructure on the fatigue properties of WAAM Ti-6Al-4V. Published studies on WAAM Ti-6Al-4V have shown that defects are the preferred fatigue crack initiation sites that can lead to fatigue strength reduction (Wang *et al.* 2013; Biswal *et al.* 2019). Biswal et al. investigated the effect of designed porosity on fatigue performance of WAAM Ti-6Al-4V built by the oscillation strategy. Fatigue strength of porosity specimens was reduced by a factor of 1.5 compared to specimens without porosity (Biswal *et al.*, 2019).

Fatigue crack propagation rate is mainly affected by the microstructure features and process induced residual stresses; defects and surface roughness have no or negligible effect. Our previous study on single bead build WAAM Ti-6Al-4V (Zhang *et al*. 2017) found that crack growth rate was lower when crack propagated across the build layers comparing to crack growing parallel to layers, albeit the small difference. In contrast, Xie *et al*. (2018) showed crack growth rate being 5% lower when crack grew in parallel with the build layers, and related this to the continuous interaction of the crack tip with the columnar β grains, which resulted in greater resistance to crack growth rate repeatedly. On the other hand, Lorant (2010) did not find any anisotropy in the crack growth rate property in WAAM Ti-6Al-4V. Studies on this front so far [Zhang *et al*. 2017, Xie *et al*. 2018, Lorant 2010] are inconclusive in terms of crack growth rate anisotropy in WAAM Ti-6Al-4V. The difference in these studies is likely caused by the competing mechanisms from microstructure and residual stress. Furthermore, crack growth rate properties in Zhang *et al.* (2017) were only investigated with the material by single bead deposition method, which is limited to the maximum build thickness of 7 mm. For thicker structures, parallel and oscillation build methods are currently available. Hence, it is important to study the

effect of different deposition methods on fatigue crack growth rate and the property anisotropy.

This paper is focused on the material properties crucial to structural integrity and durability of WAAM Ti-6Al-4V produced by different deposition methods, which are the influence of defects on fatigue crack initiation and effect of microstructure on fatigue crack growth rate. The key objectives are: (a) to develop predictive methods for porosity defect and its effect on fatigue life taking into account of the defect size, location, distribution and current NDT capabilities; (b) to study fatigue crack propagation behaviour in two build methods and two crack orientations, in order to provide crack growth rate properties for damage tolerance design for this new alloy.

METHODS

(1) Experimental design

WAAM Ti-6Al-4V material was deposited using a grade-5 Ti-6Al-4V wire with a wire diameter 1.2 mm, using a HiVE machine that had a Fronius Plasma 10 module attached to a rotator, wire feeder and the wire spool around the plasma torch. The base plate was a hot-rolled Ti-6Al-4V of 12 mm thickness and was clamped to a rigid steel backing block during deposition. Heat from the substrate was extracted by a water-cooled backing plate. Argon gas of 99.99% purity was used as shielding gas (placed ahead of the torch and as well as the trailing end of the torch), directed precisely at the melt pool to avoid oxidation.

The test program to study the effect of porosity on high cycle fatigue consisted of two batches of WAAM Ti-6Al-4V specimens, (1) material was deposited using the standard processing route as shown in Fig. 1(a), referred to as reference group, (2) using contaminated wires to deposit the specimen gauge section as shown in Fig. 1(b), referred to as porosity group. The wire was contaminated using water displacement 40th formula (WD-40®), details can be found in (Biswal *et al.*, 2019). The chemical composition (% by weight) of all the influential elements in both the batches was within the permissible limits laid out by ASTM F3302-18.

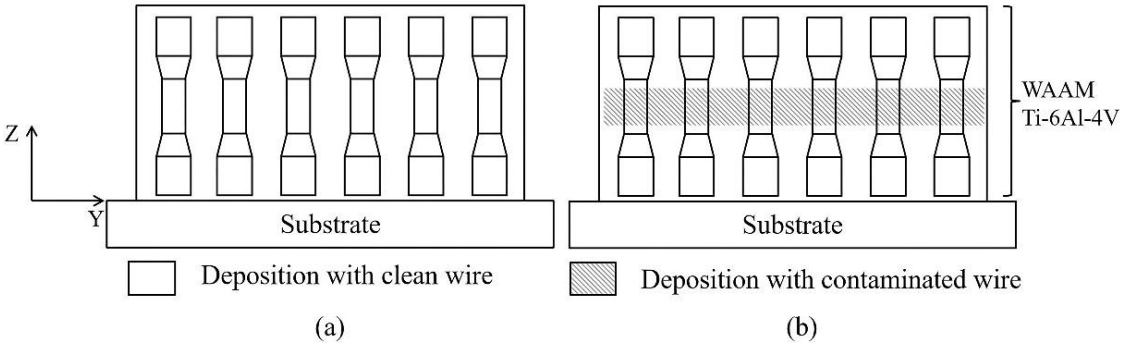

Fig. 1 Specimen extraction: (a) reference specimens, (b) porosity specimens.

The test programme to study fatigue crack growth behavior was performed using two different material deposition methods, i.e. parallel path and oscillation builds. Schematic of the two deposition methods is shown in Fig. 2(a). Two WAAM Ti-6Al-

4V walls were deposited, one by the parallel and one by oscillation method, both are of 450 mm length, 150 mm height and 22 mm thick as shown in Fig. 2(b). After the deposition, the walls were separated from the substrate plate and compact tension samples were extracted. Fig. 2(b) shows the schematic of the two sample orientations with respect to the build layers.

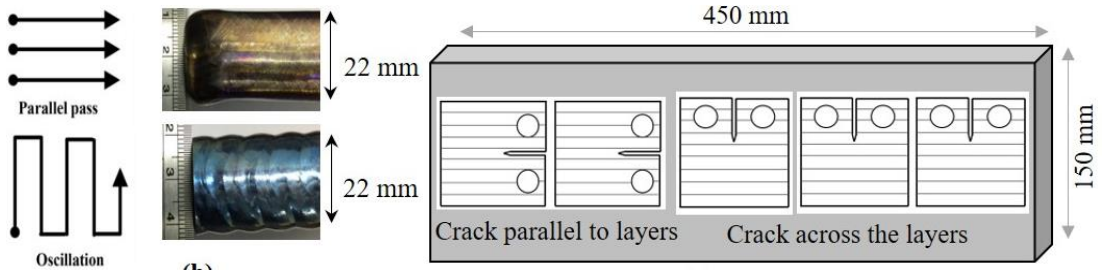

Fig. 2 (a) Two different deposition methods for building two WAAM Ti-6Al-4V walls, (b) schematic of compact tension sample extraction and crack orientations

(2) Specimen design and testing method

Tensile and fatigue testing

Flat tensile specimens were machined according to ASTM E8 as shown in Fig. 3(a). Load controlled fatigue test specimens were extracted from the porosity wall in vertical orientation with respect to the build direction and machined according to ASTM E466 standard as shown in Fig. 3(b). Three specimens were subjected to interrupted fatigue-tomography testing which have been referred to as Fatigue-Tomography (FT) specimens FT-1, FT-2 and FT-3 while the remaining specimens were used to develop the S-N curves with and without porosity defects. Specimen FT-1 was subjected to interrupted fatigue test with six X-ray computed tomography (CT) measurements taken at the test start and at suitable intervals during the fatigue test. The remaining two specimens, i.e. FT-2 and FT-3, were scanned before the start of the test and fatigue tested till failure.

The interrupted fatigue-tomography test set-up consisted of two units: a 50 kN load controlled fatigue test unit (Shimadzu) and an X-ray CT scanning unit (X TH 160 system, Nikon Metrology). The entire gauge section (5 mm diameter and 10 mm length) of the specimen was scanned by the X-ray CT to map the initial porosity distribution. Specimen FT-1 was then fatigue tested at an applied stress amplitude of 315 MPa, stress ratio of 0.1 and frequency of 20 Hz for 2×10^4 cycles which is approximately 65% of the expected fatigue life of the specimen based on published test results (Biswal *et al.*, 2019). At this point the fatigue test was interrupted to perform X-ray CT scanning, following which the fatigue test was resumed. Subsequent fatigue tests were interrupted at every few thousand cycles to perform X-ray CT scans. All the X-ray CT scans were conducted at an accelerating voltage of 120 kV, current of 58 µA and voxel size of 20 µm (effective pixel size of 10 µm). Exposure time was set at 500 ms while capturing 1583 projections (rotation step size

0.22°), which resulted in each interrupted scan time of approximately 50 minutes. The scanned files were analysed using Volume graphics® software (VG Studio Max 2.2).

Fatigue crack growth testing

For each deposition strategy, five compact tension samples were extracted, two for crack parallel to the layers and three for crack perpendicular to the layers. The compact tension samples were extracted from the mid thickness of the wall. Fig. 3(d) shows the geometry and dimension of the compact tension sample. Crack growth testing was performed according to the ASTM E647 standard, at a maximum load of 3 kN, load ratio 0.1 and 10 Hz frequency.

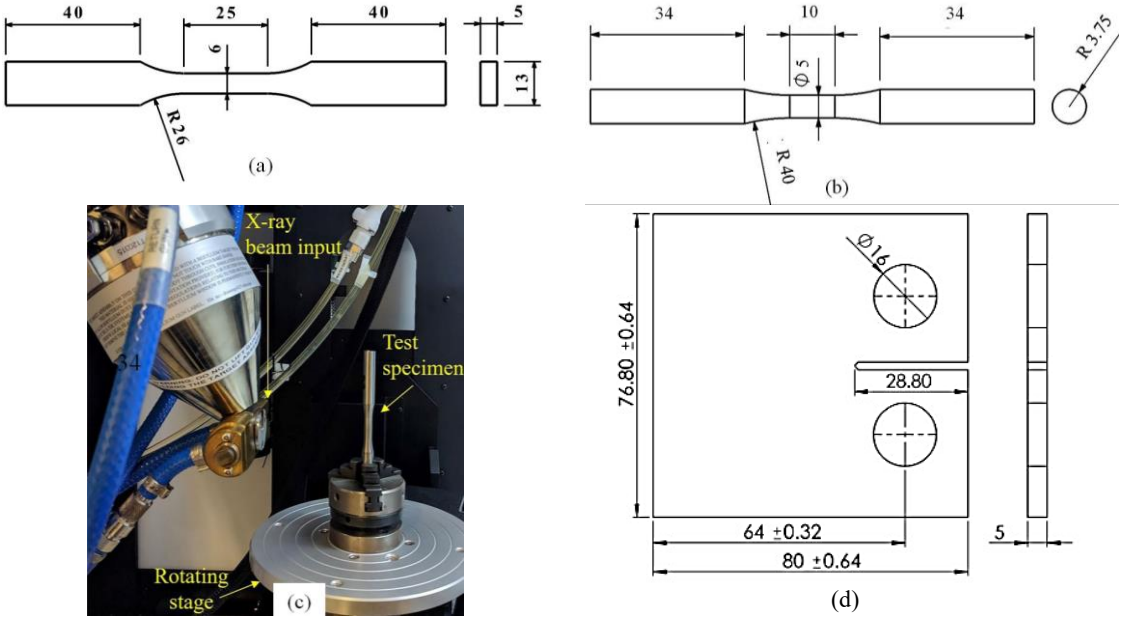

Fig. 3 Specimens for (a) tensile test, (b) load-controlled fatigue test; (c) X-ray computer tomography set-up for porosity mapping (test facility at TU Dortmund, Germany); (d) compact tension specimen and dimensions.

RESULTS AND DISCUSSION

(A) Effect of porosity defects on high cycle fatigue

Porosity Analysis

The size distribution of gas pores was studied using the X-ray CT scans and it was evident that the reference group specimens can consist of micron sized pores (62±23µm). In contrast, the size of gas pores in the porosity group specimens (206±80µm) were found to be much larger. Further, the X-ray CT scans showed that the gas pore morphology in both the groups was near spherical and the spatial distribution was isolated from each other, such that material density was found to be 99.99% and 99.96% in the reference and porosity groups respectively.

Tensile and Fatigue Tests

Tensile test results (Fig. 4a) showed that the tensile strength and yield strength of both the groups were comparable (tensile strength 859±4 MPa and yield strength 802±7 MPa). However, the uniform elongation measured in the two groups was widely separated (porosity group 4% and reference group 10%). Similarly, the S-N test data (Fig. 4b) showed that the fatigue limit i.e. applied stress range for a life of 10^7 cycles, was 540 MPa for the reference group and 360 MPa for the porosity group at an applied stress ratio of 0.1. This indicates that WAAM Ti-6Al-4V has a notch fatigue factor of 1.5 and notch sensitivity of 0.5 for spherical gas pores. It is worth mentioning that the fatigue performance of as-built (i.e. non-heat treated, polished) WAAM Ti-6Al-4V specimens was close to the wrought and HIPed AM Ti-6Al-4V alloy.

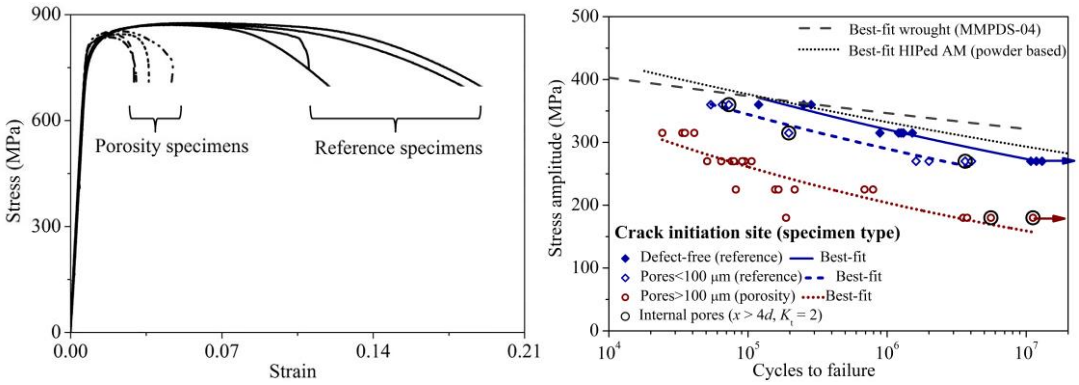

Fig. 4 Results of (a) static tensile test, (b) fatigue test at applied stress ratio 0.1; Reference data and sources: wrought (MMPDS, 2008); powder fusion AM - hot isostatically pressed (HIP) AM: selective laser melting (Bagehorn *et al.*, 2017; Kahlin *et al.*, 2017); electron beam melting (Ackelid *et al.*, 2009; Brandl *et al.*, 2011; Hrabe *et al.*, 2015; Kahlin *et al.*, 2017; Shui *et al.*, 2017).

Interrupted fatigue-tomography test

Interrupted fatigue-tomography test (Fig. 5) showed tortuous cracks originated preferentially at sub-surface pores that grew towards the nearest free surface. This can be explained by the higher values of the stress concentration factor (SCF) for sub-surface pores, which is at least 25% higher than that of an internal pore and depends on the distance of the pore to the specimen free surface. The location of the cracks were found to be at the mid-riff section of the pores as shown in Fig. 5(c), so the critical sub-surface pores were expanding under cyclic loads.

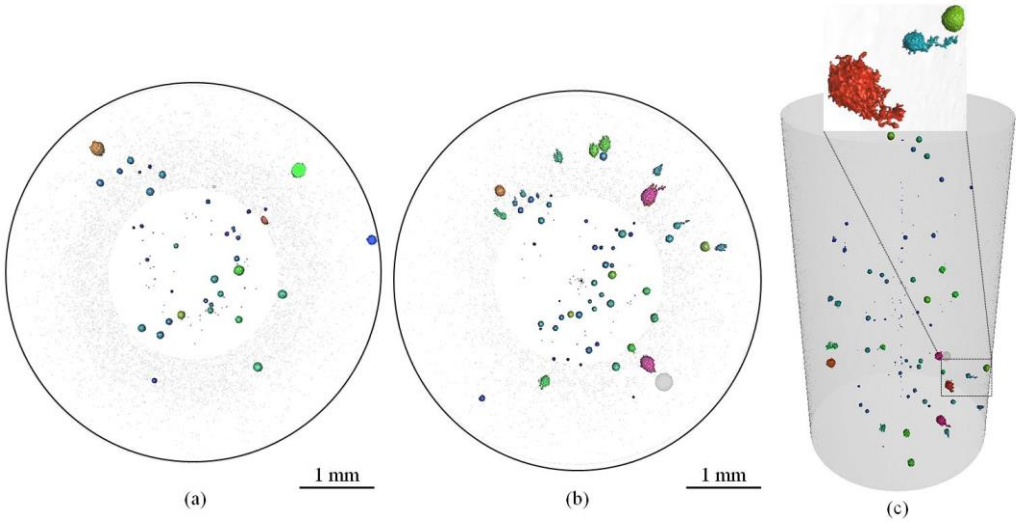

Fig. 5 Images of interrupted fatigue-tomography test showing the overall cross-sectional (or top view) of the X-ray CT scan taken at: (a) zero cycle, just before the fatigue test, (b) 3.2×10^4 cycles (specimen failed at 32380 cycles), (c) three dimensional view of the scanned section at 3.2×10^4 cycles.

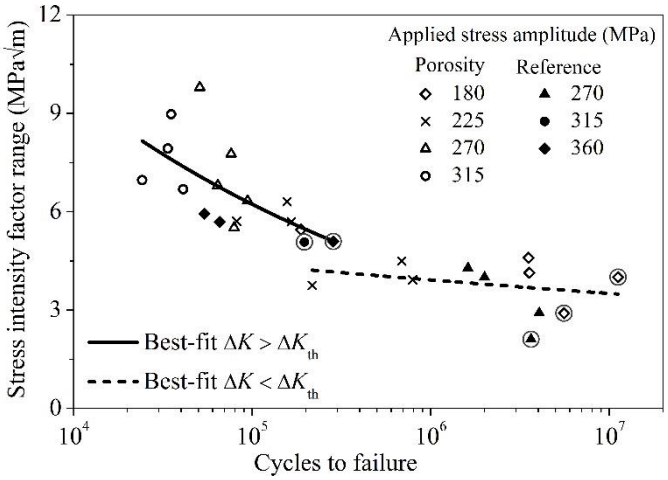

Fig. 6 Correlation between fatigue life and stress intensity factor range (SIF range) for porosity defects tested in this study (SIF range is calculated using the Murakami's equation, Eq. 1). Note: encircled data points denote crack initiation at internal pores; the majority failed by cracks initiating from sub-surface pores.

Stress intensity factor range applied to gas pore defects

Since the applied stress range and the porosity defect size are both play an important role in determining the fatigue performance, the stress intensity factor (SIF) range was used to correlate the fatigue test results. According to Murakami's model (Murakami and Endo, 1986), a spherical gas pore can be treated as a planar crack of size equal to the square root of the projected area of the pore. Stress intensity factor range was calculated by Murakami's equation as shown here by Eq. (1).

$$\Delta K = C \times \Delta\sigma\sqrt{\pi\sqrt{area}} \qquad \text{Eq (1)}$$

where ΔK is the stress intensity factor range, $\Delta\sigma$ the applied stress range, √area the square root of the projected area of the pore, and parameter C is 0.5 for internal defects and 0.65 for surface defects.

Fatigue test result presented in Fig. 4(b) have been re-plotted as a relation of ΔK vs. N in Fig. 6 showing a much better correlation between the fatigue life and the fracture mechanics parameter.

(B) Fatigue crack growth behaviour

Measured fatigue crack growth rates (FCGR) for the parallel path and oscillation wave builds are shown in Fig. 7, for two different crack orientations, and compared with traditional method processed Ti-6Al-4V, i.e. cast, wrought (mill annealed) and wrought (beta annealed). Numbers in the figure legends represent repeated fatigue tests for each case.

Crack orientation

When crack propagated in parallel to the WAAM build layers, the influence of different deposition method on FCGR is negligible, as shown in Fig. 7a. In this crack orientation, crack growth rate was lower than that of the wrought material (mill annealed), but greater than that of casting and beta annealed before ΔK reached 18 MPa√m; beyond this value, crack growth rate in WAAM and beta annealed conditions are similar.

When crack growth was across the WAAM layers, Fig. 7b, WAAM Ti-6Al-4V showed lower crack growth rate compared to the wrought and similar crack growth rates as the cast and the beta annealed. The oscillation build had much lower crack growth rate in two tests, but another test had much higher growth rate, which is similar to that from the parallel build. Therefore, it is not yet conclusive for the oscillation wave build; further research is required on the competing mechanisms of microstructure and residual stress; the latter depends on specimen extraction location. If we analyse the crack propagation with respect to the columnar prior-β grain orientation, the crack in this orientation propagated in parallel with the columnar prior-β grain orientation.

The role of the macro- and micro-structure and morphology of the microstructural constituents can play an important role on the fatigue crack behaviour of a material. In Ti-6Al-4V, size and morphology of α lath are the primary microstructural parameters that control the plastic zone ahead of the crack tip, therefore the fatigue crack growth rate (Han *et al*. 2016; Tan *et al*. 2018). If we analyse the crack growth rate with respect to the microstructure, the low crack growth rate in the cast and beta annealed materials is owing to the presence of fully lamellar and lamellar plus basket weave microstructure respectively. On the other hand, the mill annealed wrought material consists of duplex microstructure with near equiaxed grains, and consequently leads to faster crack growth rate.

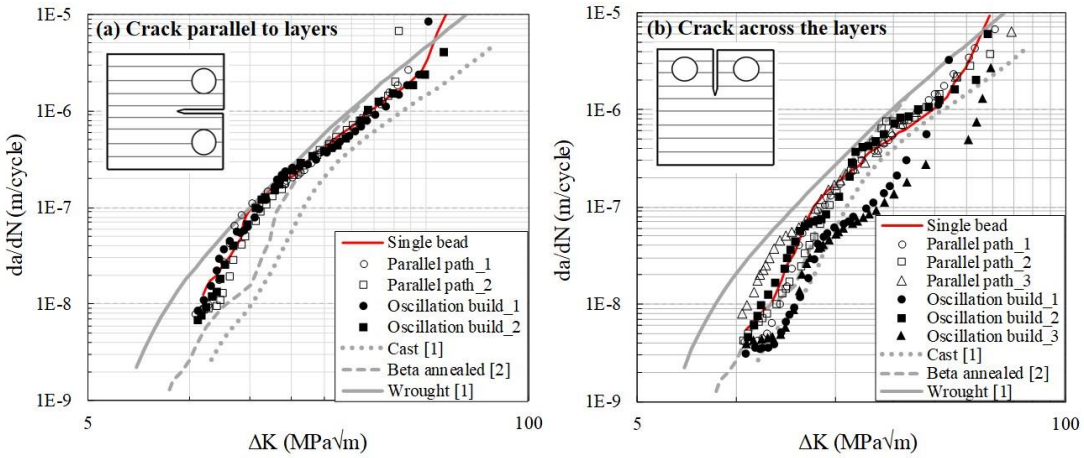

Fig. 7: Fatigue crack growth rates and comparison of two different build methods: (a) crack propagating parallel to layers, (b) crack across the layers

Build methods and effect on property anisotropy

Degrees of anisotropy in fatigue crack growth rate for the parallel path and oscillation wave built samples are presented in Fig. 8. The parallel build samples did not show considerable anisotropy in crack growth rate, with only a small difference between the two crack orientations at ΔK values of 12-15 MPa√m, Fig. 8a. The oscillation build samples showed significant anisotropy in Fig. 8b, where samples with crack crossing the layers showed much lower crack growth rate, except the Test No. 2.

The lower crack growth rate in the across layer samples is thought to be associated with the crack propagating through the layer banding along the build direction. Ho *et al*. (2019) presented detailed microstructure analysis of single path build WAAM Ti-6Al-4V showing that the banding appearance regions are either heat affected zones (HAZ) or segregation areas that are formed due to repeated thermal cycling during the deposition process. The study also showed that the top of each HAZ zone is associated with very fine α packets with very fine spacing along the build direction, resulting in more resistance to crack propagation across the layers comparing to crack growth in parallel to the layers. For the crack across the layer specimens, the crack tip passes through each layer band, so it continuously encounters fine α packets in the HAZ and segregation zones that will slow down the crack growth rate. Detailed microstructure analysis of layer banding can be found in (Ho *et al*. 2019). It remains to be studied whether the parallel and oscillation deposition methods have also influenced the HAZ and segregation zones. The absence of anisotropic crack growth rate in the parallel path build samples might be associated with the very low or absence of HAZ and segregation zones. The anisotropic crack growth rate observed in the oscillation build samples might be due to the presence of pronounced HAZ and segregation zones and the crack propagating through these regions in crack across the layer samples. Hence, a lower crack growth rate is observed.

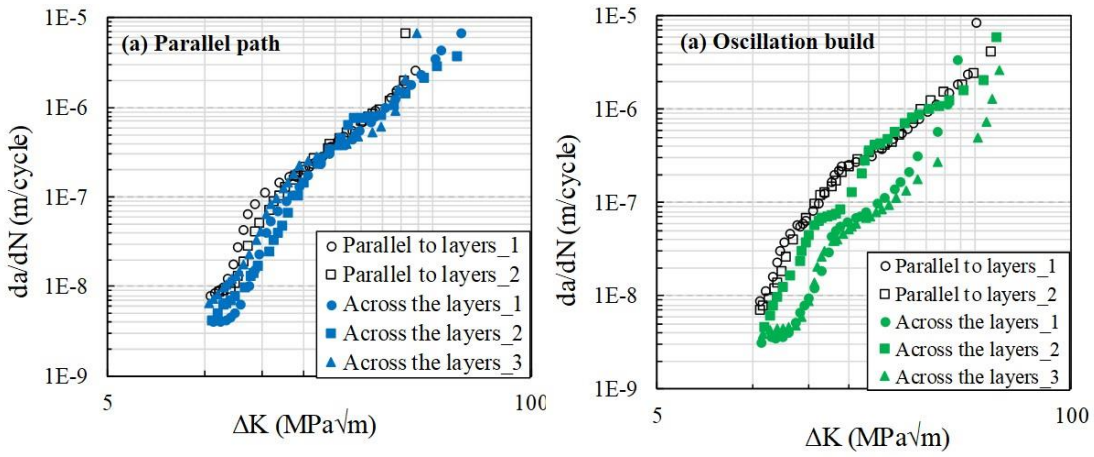

Fig. 8: Crack growth rates in both crack orientations in (a) parallel and (b) oscillation builds.

ACKNOWLEDGEMENT

The work was supported by the industrial partners through the WAAMMat programme. We also acknowledge UK Engineering and Physical Sciences Research Council (EPSRC) for funding through grants EP/K029010/1 and EP/R027218/1.

CONCLUSIONS

- Embedded porosity defects were introduced to the specimen gauge section by using contaminated wires during the additive manufacturing. X-ray computer tomography scans showed spherical pores distributed scarcely (i.e. isolated from each other). Interrupted fatigue-tomography tests showed preferential crack initiation from the near surface pores; the subsequent crack growth was directed towards the nearest free surface.

- Porosity defects did not reduce the tensile strengths, however the ductility was reduced from 10% to 4% and fatigue strength (in terms of cyclic stress range at stress ratio 0.1) was reduced from 540 MPa (reference, defect-free) to 360 MPa.

- A good correlation was found between the fatigue life and the stress intensity factor (SIF) range of the crack initiating defect, where the SIF for pore geometry was calculated using Murakami's equation.

- Fatigue crack growth rate in WAAM Ti-6Al-4V is lower than the mill annealed wrought but higher than the β annealed wrought and casting materials.

- The parallel path deposition method showed higher crack growth rate than the oscillation build when crack is across the layers. However, there is virtually no difference between the two build methods when crack is parallel to the layers.

- Anisotropic fatigue crack growth rate was observed only for the oscillation build, whereas the parallel path build had almost isotropic crack growth rates between the two major crack orientations.

REFERENCES

Åkerfeldt, P., Antti, M. L. and Pederson, R. (2016) 'Influence of microstructure on mechanical properties of laser metal wire-deposited Ti-6Al-4V', *Materials Science and Engineering A*., 674, pp. 428–437.

Bagehorn, S., Wehr, J. and Maier, H. J. (2017) 'Application of mechanical surface finishing processes for roughness reduction and fatigue improvement of additively manufactured Ti-6Al-4V parts', *International Journal of Fatigue*., 102, pp. 135–142.

Bermingham, M. J., Kent, D., *et al.* (2015) 'Controlling the microstructure and properties of wire arc additive manufactured Ti-6Al-4V with trace boron additions', *Acta Materialia*., 91, pp. 289–303.

Biswal, R., Zhang, X., *et al.* (2019) 'Criticality of porosity defects on the fatigue performance of wire + arc additive manufactured titanium alloy', *International Journal of Fatigue*., 122, pp. 208–217.

Brandl, E., Palm, F., *et al.* (2011) 'Mechanical properties of additive manufactured titanium (Ti-6Al-4V) blocks deposited by a solid-state laser and wire', *Materials and Design*, 32(10), pp. 4665–4675.

Colegrove, P. A., Donoghue, J., *et al.* (2017) 'Application of bulk deformation methods for microstructural and material property improvement and residual stress and distortion control in additively manufactured components', *Scripta Materialia*., 135, pp. 111–118.

Günther, J., Krewerth, D., *et al.* (2016) 'Fatigue life of additively manufactured Ti-6Al-4V in the very high cycle fatigue regime', *International Journal of Fatigue*, 94, pp. 236–245.

Han, F., Tang, B., *et al.* (2016), 'Cyclic softening behavior of Ti–6Al–4V alloy at macro and micro-scale', Mater. Lett. 185, pp. 115–118.

Ho, A., Zhao, H., *et al.* (2019), 'On the origin of microstructural banding in Ti-6Al4V wire-arc based high deposition rate additive manufacturing', Acta. Mat. 166, pp. 306-323.

Hönnige, J. R., Colegrove, P. A., *et al.* (2018) 'Residual stress and texture control in Ti-6Al-4V wire + arc additively manufactured intersections by stress relief and rolling', *Materials and Design*., 150(2017), pp. 193–205.

Hrabe, N., Gnaupel-Herold, T. and Quinn, T. (2015) 'Fatigue properties of a titanium alloy (Ti-6Al-4V) fabricated via electron beam melting (EBM): Effects of internal defects and residual stress', *International Journal of Fatigue*, 94, pp. 202–210.

Kahlin, M., Ansell, H. and Moverare, J. J. (2017) 'Fatigue behaviour of notched additive manufactured Ti6Al4V with as-built surfaces', *International Journal of Fatigue*., 101, pp. 51–60.

Leung, C. L. A., Marussi, S., *et al.* (2018) 'In situ X-ray imaging of defect and molten pool dynamics in laser additive manufacturing', *Nature Communications*., 9(1), pp. 1–9.

Lorant, E. (2010), 'Effect of microstructure on mechanical properties of Ti-6Al-4V structures made by additive layer manufacturing', MSc thesis, Cranfield University.

Lu, S. L., Tang, H. P., *et al.* (2015) 'Microstructure and mechanical properties of long Ti-6Al-4V rods additively manufactured by selective electron beam melting out of a deep

powder bed and the effect of subsequent hot isostatic pressing', *Metallurgical and Materials Transactions A*, 46(9), pp. 3824–3834.

Metallic Materials Properties Development and Standardization (MMPDS-04), Battelle Memorial Institute; 2010.

Murakami, Y., Endo, M., 'Effects of Hardness and Crack Geometries on ΔK_{th} of Small Cracks Emanating from Small Defects', Mechanical Engineering Publications; 1986.

Seifi, M., Salem, A., *et al.* (2017) 'Defect distribution and microstructure heterogeneity effects on fracture resistance and fatigue behavior of EBM Ti-6Al-4V', *International Journal of Fatigue*., 94, pp. 263–287.

Shui, X., Yamanaka, K., *et al.* (2017) 'Effects of post processing on cyclic fatigue response of a titanium alloy addtively manufactured by electrom beam melting', *Materials Science & Engineering A*., 680, pp. 239–248.

Sterling, A. J., Torries, B., *et al.* (2016) 'Fatigue behavior and failure mechanisms of direct laser deposited Ti-6Al-4V', *Materials Science and Engineering A*., 655, pp. 100–112.

Svensson, M. and Ackelid, U., (2009) 'Additive manufacturing of dense metal parts by electron beam melting'. In: Material science and technology conference, pp. 2711–9.

Tammas-Williams, S., Withers, P. J., *et al.* (2017) 'The influence of porosity on fatigue crack initiation in additively manufactured titanium components', *Scientific Reports*., pp. 1–13.

Tan, C., Sun, Q., *et al.* (2018), 'Cyclic deformation and microcrack initiation during stress controlled high cycle fatigue of a titanium alloy', *Material Science and Engineering. A*. 711, pp. 212–222.

Wang, F., Williams, S., *et al.* (2013) 'Microstructure and mechanical properties of wire and arc additive manufactured Ti-6Al-4V', *Metallurgical and Materials Transactions A: Physical Metallurgy and Materials Science*, 44(2), pp. 968–977.

Williams, S. W., Martina, F., *et al* (2016) 'Wire + Arc Additive Manufacturing'Materials Science and Technology., 32 (7)., pp. 641-647.

Wycisk, E., Solbach, A., *et al.* (2014) 'Effects of defects in laser additive manufactured Ti-6Al-4V on fatigue properties', *Physics Procedia*., 56, pp. 371–378.

Xie, Y., Gao, M., *et al.* (2018) 'Anisotropy of fatigue crack growth in wire arc additive manufactured Ti-6Al-4V', *Material Science and Engineering A*. 709, pp. 265–269.

Zhang, J., Wang, X., *et al.* (2016) 'Fatigue crack propagation behaviour in wire+arc additive manufactured Ti-6Al-4V: Effects of microstructure and residual stress', *Materials and Design*., 90, pp. 551–561.

Zhang, X., Martina, F., et al. (2017) 'Fatigue Crack Growth in Additive Manufactured Titanium: Residual stress control and life evaluation method development', *29th ICAF Symposium – Nagoya*, 7–9 June 2017.

High cycle fatigue and fatigue crack growth rate in additive manufactured titanium alloys

Xiang Zhang [1], Abdul Khadar Syed [1], Romali Biswal [1]
Filomeno Martina [2], Jialuo Ding [2], Stewart Williams [2]
[1] *Coventry University, Coventry, United Kingdom*
[2] *Cranfield University, Cranfield, United Kingdom*

The Wire+Arc Additive Manufacture (WAAM) can produce large area metal parts in terms of metre-scale, with higher deposition rate compared to the powder bed fusion AM processes. The process also offers lead time reduction and much lower buy-to-fly ratio compared to forgings. Research is much needed in the fatigue and fracture properties for qualification of additive manufactured aircraft components.

WAAM Ti-6Al-4V alloy has been tested and modelled, focusing on two key areas of structural integrity: (1) high cycle fatigue and the effect of defects; (2) fatigue crack growth rates and effects of heterogeneous microstructure and process induced residual stresses. The key objectives are: (a) to develop predictive methods for defect tolerant fatigue assessment taking account of the defect size, location, distribution and current NDT capabilities; (b) to study fatigue crack propagation behaviour in two crack orientations with respect to the material build direction, to provide crack growth rate and fracture toughness properties for damage tolerance design considerations.

(1) Effect of defects on high cycle fatigue performance

Interrupted fatigue-tomography experiments were performed on specimens with porosity defects embedded in the gauge section. Defects were embedded intentionally using contaminated wires. In practice, feedstock may get contaminated causing pores of considerable size in the material. Static strength was comparable to the reference group without porosity, but both ductility and fatigue strength were significantly reduced owing to the presence of defects. S-N data could not correlate the test results owing to different pore sizes and at different applied stresses (*Figure 1a*). Using the fracture mechanics and Murakami's equation for stress intensity factor of embedded pores [1], good correlation was found between the fatigue life and stress intensity factor of the crack initiating defects (*Figure 1b*). Critical pore diameter was found to be between 50-100 micrometers. Method from El-Haddad et al. [2] is used to establish the Kitagawa-Takahashi diagram for criticality analysis of porosity defects.

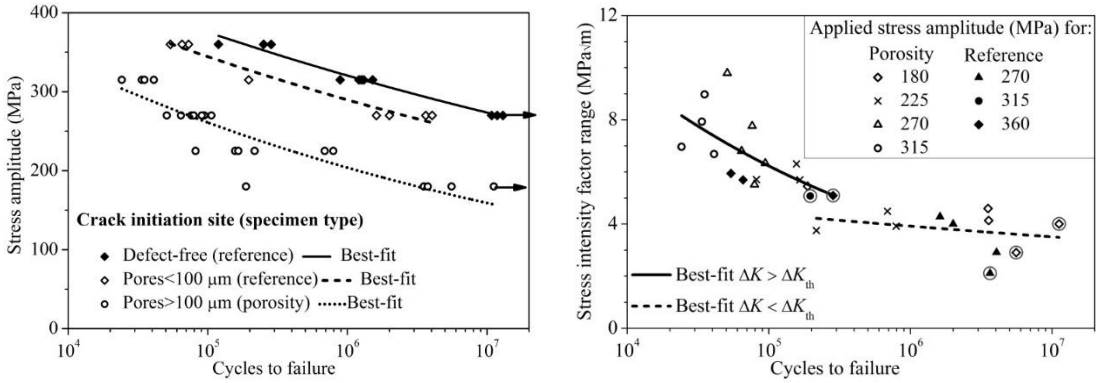

Figure 1. (a) S-N data of control and porosity specimens, devided by porosity size and location; (b) stress intensity factor range vs. fatigue life, showing good correlation with critical pore size

(2) Fatigue crack growth rate

Compact tension specimens made by three different WAAM build strategies with two crack orientations, i.e. crack either across or parallel to the deposited layers. Residual stress in the large build wall and small laboratory coupons were determined by the neutro diffraction and contour methods. Microstructure and texture characteristics and their influence on the crack growth rates and path were investigated. A predictive model based on linear elastic fracture mechanics has been developed.

Key findings are: (a) residual stress in small C(T) specimen is very low (below 100 MPa), *Figure 2a*, despite being extracted from a much larger build wall that contained much higher residual stress (maximum tensilte residual stress is around 600-800 MPa depending on the build size and location to the substrate palte). Fatigue crack growth rate measured by small samples is mainly affected by the microstructure morphologies (*Figure 2b*); residual stress effect is neglegible. (b) Life prediciton method for large parts: residual stress must be considered and can be accounted for by the effective *R* ratio term; fatigue crack

growth rate (FCGR) should be considered as material's intrinsic property, which is measured by small samples with neglegible residual stress. (c) compared to traditional manufacturing methods, fatigue crack growth rates in as-built WAAM Ti-6Al-4V is lower than the mill annealed, similar to the beta annealed, and slightly greater than cast conditions, making the WAAM a viable additive manufacture process to produce aerospace titanium alloys for damage tolerant design.

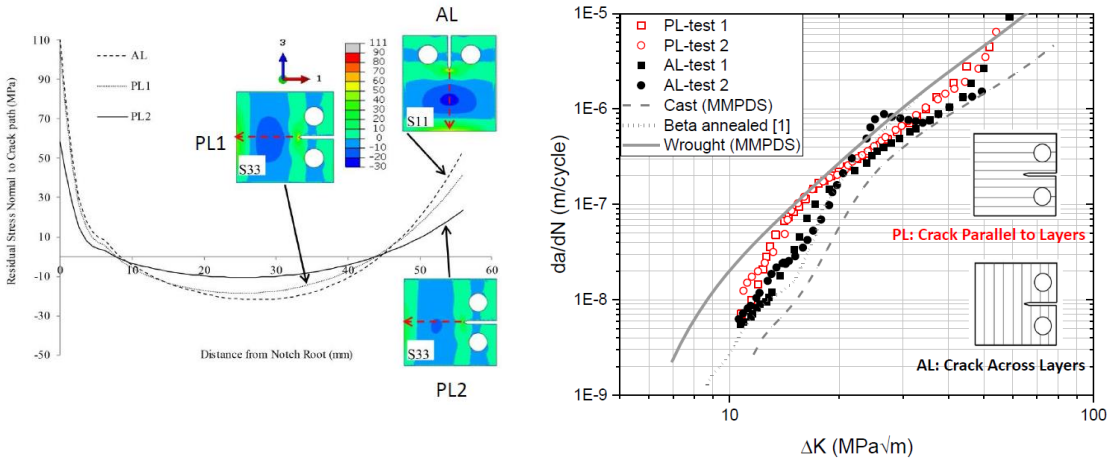

Figure 2. (a) residual stresses in compact tension specimens (maximum stress is about 100 MPa at notch root; AL: crack across additive layers; PL: crack parallel to layers); (b) fatigue crack growth rates in single bead built; difference in crack growth rate at lower stress intensity factor range is owing to the difference in microstructure morphology.

References

[1] Murakami Y. Metal fatigue: Effects of Small Defects and Nonmetallic Inclusions. 1st ed. Chapter 4. Elsevier; 2002

[2] El Haddad MH, Topper TH, Smith KN. Prediction of non-propagating cracks. Eng Fract Mech 1979; 11: 573–84.

Keywords*: additive manufacturing, high cycle fatigue, defects, fatigue crack growth rate, microstructure, residual stress*

https://dspace.org/

High cycle fatigue and fatigue crack growth rate in additive manufactured titanium alloys

Zhang, Xiang; Syed, Abdul Khadar; Biswal, Romali; Martina, Filomeno; Ding, Jialuo ...

2019-07-03
Springer
https://doi.org/10.1007/978-3-030-21503-3_3
Zhang X, Syed AK, Biswal R, et al., (2019) High cycle fatigue and fatigue crack growth rate in additive manufactured titanium alloys, In: ICAF 2019 – Structural Integrity in the Age of Additive Manufacturing. Proceedings of the 30th Symposium of the International Committee on Aeronautical Fatigue, June 2-7, 2019, Krakow, Poland. pp. 31-42

Downloaded from a DSpace repository. https://dspace.org/